Future Cities and Environment
ISSN 2363-9075 Volume 12 (2026)

https://doi.org/10.70917/fce-2026-019

Article

Structural Investigation of Fatigue Behavior in Corroded Subsea Pipelines for CO_2 Transportation using the Strain–Life Approach

Aprianur Fajri [1,2,3], Indri Yaningsih [1,*], Aditya Rio Prabowo [1,2], Ristiyanto Adiputra [4], Nurul Muhayat [1], Rahman Wijaya [1], Eko Prasetya Budiana [1], Godlisten Gladstone Kombe [5], Buruhan Haji Shame [6] and Svitlana Onyshchenko [7]

[1] Department of Mechanical Engineering, Universitas Sebelas Maret, Surakarta 57126, Indonesia; (A.F; https://orcid.org/0009-0000-1759-2397); (I.Y; https://orcid.org/0000-0001-7124-0261); (A.R.P; https://orcid.org/0000-0001-5217-5943); (N.M; https://orcid.org/0000-0002-1086-7826); (R.W; https://orcid.org/0009-0008-6060-5286); (E.P.B; https://orcid.org/0000-0002-7811-779X).
[2] Laboratory of Designs and Computational Mechanics, Faculty of Engineering, Universitas Sebelas Maret, Surakarta 57126, Indonesia.
[3] Department of Manufacturing Engineering Technology, Akademi Inovasi Indonesia, Salatiga 50721, Indonesia.
[4] Research Center for Hydrodynamics Technology, National Research and Innovation Agency (BRIN), Surabaya 60117, Indonesia; (R.A; https://orcid.org/0000-0003-3630-9432).
[5] Department of Petroleum and Energy Engineering, The University of Dodoma, Dodoma 41218, Tanzania; (G.G.K; https://orcid.org/0000-0002-7527-5653).
[6] The Ministry of Infrastructure, Communication, and Transportation, Zanzibar 70470, Tanzania; (B.H.S; https://orcid.org/0009-0001-8554-8766).
[7] Department of Fleet Operation and Technology of Sea Transportation, Odesa National Maritime University, Odesa 65029, Ukraine; (S.O; https://orcid.org/0000-0002-7528-4939).
* Correspondence author: indriyaningsih@staff.uns.ac.id

Abstract: The subsea CO_2 transport pipelines, which are closely related to environmentally sound technology under Sustainable Development Goal (SDG) 17, are subjected to cyclic loading from ocean currents, wave-induced forces, internal pressure fluctuations, and start–stop operating cycles. In harsh marine environments, corrosion may reduce pipe-wall strength and create local defects that promote fatigue crack initiation. These cracks may subsequently propagate under cyclic loading, leading to structural failure. This study investigates the fatigue crack initiation life of corroded subsea steel pipelines for CO_2 transportation using an integrated local strain–life (ε–N) framework. The framework combines nonlinear finite element analysis, the Coffin–Manson–Basquin relation, and the Smith–Watson–Topper mean-stress correction. The modeled pipeline has an outer diameter of 300 mm, a wall thickness of 20 mm, and a length of 1,800 mm, with API 5L X65 steel adopted as the pipeline material. Rectangular corrosion defects with varying depth, length, and width are considered, while the internal pressure ranges from 0 to 20 MPa. Fully reversed cyclic bending is applied with a stress ratio of $R = -1$. The finite element results are used to extract local stress–strain responses at the corrosion defect, which are then used to predict fatigue crack initiation life. The results show that corrosion defects produce pronounced strain localization, in contrast to the relatively uniform strain distribution in intact pipelines. Corrosion depth is the most critical geometric parameter because it directly reduces the effective wall thickness and increases the local cyclic strain amplitude. Corrosion length affects fatigue life through strain redistribution: short defects behave as severe strain concentrators, whereas longer defects reduce peak strain under displacement-controlled bending. Corrosion width has a secondary effect by modifying the circumferential constraint. Internal pressure further reduces fatigue life by introducing tensile membrane stress and a non-zero local mean stress. Overall, fatigue crack initiation in corroded subsea CO_2 pipelines is governed by the coupled effects of thickness reduction, strain localization, circumferential

constraint, and pressure-induced mean stress. These findings highlight the importance of local strain-based assessment for reliable pipeline integrity evaluation.

Keywords: CO_2 transport pipelines; environmentally sound technology; corrosion defect; fatigue analysis; FEM; strain-life approach

Nomenclature

$2N_f$	number of strain reversals to failure
b	fatigue strength exponent
c	fatigue ductility exponent
d	corrosion depth (mm)
D	outer diameter (mm)
E	elastic modulus (GPa)
k	number of load blocks in the spectrum
l	corrosion length (mm)
L	specimen length (mm)
l_e	max. element length measured at pipe surface (mm)
n_i	number of applied cycles at load level i
N_i	number of cycles to failure at load level i
P	internal pressure loading (in MPa)
t	pipe thickness (mm)
t_{ef}	effective local wall thickness (mm)
w	corrosion width (mm)
ε_a	total strain amplitude
$\varepsilon_{a,e}$	elastic strain amplitude
$\varepsilon_{a,p}$	plastic strain amplitude
$\varepsilon_f^{'}$	fatigue ductility coefficient
$\sigma_f^{'}$	fatigue strength coefficient
σ_a	stress amplitude in a loading cycle (MPa)
σ_{max}	maximum stress in a loading cycle (MPa)
σ_{min}	minimum stress in a loading cycle (MPa)
σ_{UTS}	material ultimate tensile strength (MPa)
σ_y	material yield strength (MPa)

1. Introduction

Carbon capture and storage (CCS) is a key strategy for mitigating climate change by reducing carbon dioxide (CO_2) emissions through environmentally sound technologies, as indicated in Sustainable Development Goals (SDGs) 17. In CCS systems, captured CO_2 must be transported from emission sources to geological storage sites, which may be far from the capture location and are often located offshore. Therefore, CO_2 transport systems are an essential component of the CCS value chain, with subsea pipelines serving as one of the main infrastructure options for connecting capture facilities, transport networks, and storage sites (Wennersten, Sun and Li, 2015; Baig *et al.*, 2025; Fajri *et al.*, 2026).

Subsea pipelines operate in complex marine environments in which material degradation and cyclic loading may occur simultaneously. Fatigue is a dominant damage mechanism because pipelines are repeatedly exposed to ocean currents, wave-induced forces, internal-pressure fluctuations, and start–stop operating cycles. Corrosion from seawater exposure may further degrade the pipeline's mechanical response. This degradation can be promoted by high chloride ion concentrations, dissolved oxygen, biofouling, damage to protective coatings, and ineffective cathodic protection systems. Localized corrosion increases stress and strain concentrations and may accelerate fatigue crack initiation. Therefore, understanding the effects of corrosion on the fatigue life of subsea pipelines is essential for ensuring long-term structural integrity (Udonsek, Tamonodukobipi and Odokwo, 2023; Islami *et al.*, 2025; Riffat *et al.*, 2025; Riffat *et al.*, 2026; Zhou *et al.*, 2026).

Corrosion-induced deterioration of pipeline strength has been widely studied to ensure the integrity of oil, gas, and CO_2 pipelines. Localized corrosion, such as pitting or wall thinning, acts as a geometric irregularity that increases local stress and strain concentrations (Gao *et al.*, 2024; Zhou *et al.*, 2025). Under cyclic loading, this condition accelerates crack initiation and reduces fatigue life. Farhad *et al.* (2019) emphasized the importance of evaluating the local elastoplastic response around corrosion pits through elemental-to-cyclic analysis, since approaches that directly treat pits as cracks may neglect the crack-initiation stage, which can contribute significantly to fatigue life, particularly in high-cycle regimes. In addition, Talebi *et al.* (2018) showed that corrosion exposure has a stronger influence on the response and failure of pipes subjected to cyclic rather than monotonic loading. Their results indicated that cyclic creep increases and the number of cycles to failure decreases significantly in corroded pipes.

Studies on mechanical defects further confirm that geometric imperfections can degrade the cyclic response of pressurized pipes. Ezzati *et al.* (2021) reported that dents in submarine pipes significantly reduced fatigue resistance under combined internal pressure and asymmetric inelastic cyclic loading, resulting in a much lower number of cycles to failure in the defective region. These findings reinforce the importance of accurately representing defect geometry and local stress–strain behavior in pipeline integrity assessment.

Although previous studies have examined corrosion and mechanical defects in pipelines, many fatigue assessments still rely on nominal-stress or defect-severity-based approaches. These approaches are suitable when plastic deformation is negligible. However, corrosion defects may produce severe local stress and strain concentrations, resulting in cyclic plasticity near the defect region. Under such conditions, fatigue crack initiation is governed more directly by the local cyclic strain response than by the nominal stress alone.

The present study does not develop a new fatigue-damage model or finite element formulation. Instead, it integrates established methods, the Coffin–Manson–Basquin (CMB) relation, the Smith–Watson–Topper (SWT) mean-stress correction, and nonlinear finite element analysis to assess corroded subsea CO_2 transport pipelines. The originality of this work lies in its integrated application to the specific problem of pipelines, where corrosion-induced wall thinning, cyclic bending, and pressure-induced tensile membrane stress act simultaneously. By extracting local cyclic stress–strain responses directly from nonlinear FE simulations, this study provides a mechanistic interpretation of how corrosion depth, length, width, and internal pressure jointly affect strain localization, local mean stress, and predicted fatigue crack initiation life. Therefore, the contribution of the present work is primarily application-oriented and mechanistic, rather than methodological.

The combined effects of corrosion geometry and internal pressure on the strain-controlled fatigue behavior of subsea pipelines are not yet fully understood. This is important because defect geometry and operational loading may interact to alter the local cyclic strain response that governs crack initiation. Therefore, this study numerically investigates fatigue crack initiation in corroded subsea pipelines using a strain–life framework coupled with nonlinear finite element analysis. The objective is to quantify the effects of corrosion depth, length, and width, as well as internal pressure, on the local cyclic strain state and the resulting fatigue crack initiation life under cyclic bending.

2. Strain - Life Fatigue Approach

The strain–life approach was used to predict fatigue behavior under cyclic loading conditions involving local elastoplastic deformation. The relationship between cyclic strain and fatigue life is described by the CMB formulation, which combines elastic and plastic strain components, as expressed in Eqs. (1) and (2) (Basquin, 1910; Manson, 1953; Coffin Jr., 1954). For loading conditions with a non-zero mean stress, such as those caused by internal pressure, the mean-stress effect was incorporated using the SWT parameter, as expressed in Eq. (3) (Watson and Topper, 1972). The SWT parameter relates the maximum local stress to the strain amplitude.

$$\varepsilon_a = \varepsilon_{a,e} + \varepsilon_{a,p} \tag{1}$$

$$\varepsilon_a = \frac{\sigma_f^{'}}{E}\left(2N_f\right)^b + \varepsilon_f^{'}\left(2N_f\right)^c \tag{2}$$

$$\sigma_{max}\varepsilon_a = \frac{\sigma_f^{'2}}{E}\left(2N_f\right)^{2b} + \sigma_f^{'}\varepsilon_f^{'}\left(2N_f\right)^{b+c} \tag{3}$$

The SWT criterion was adopted to account for the pressure-induced tensile mean stress in the local fatigue response. In the present loading condition, internal pressure introduces a non-reversing tensile membrane stress that is superimposed on the fully reversed cyclic bending stress. Consequently, the local stress cycle at the corrosion defect becomes asymmetric even when the nominal bending load has a stress ratio of $R = -1$. Because the SWT parameter combines the maximum local stress and strain amplitudes into a single damage parameter, it is suitable for evaluating crack initiation under strain-controlled fatigue conditions with a pressure-induced tensile mean stress. Under variable-amplitude loading, fatigue damage accumulation is commonly evaluated using the Palmgren–Miner linear damage rule, as expressed in Eq. (4) (Miner, 1945). However, this study considered only constant-amplitude cyclic loading with a single load block ($k = 1$); therefore, cumulative damage from variable-amplitude loading was not evaluated.

$$\sum_{i=1}^{k} \frac{n_i}{N_i} = 1 \tag{4}$$

The fatigue evaluation in this study was limited to the crack initiation life predicted from the local cyclic strain response obtained by finite element analysis. Crack propagation was not included. This limitation is consistent with the strain–life (ε–N) methodology, which is mainly intended to evaluate the initiation stage governed by localized cyclic plasticity. Crack propagation analysis would require a fracture-mechanics-based framework that includes assumptions about initial crack size, crack shape, stress intensity factor, crack growth direction, and material crack-growth parameters. Therefore, the fatigue lives reported in this study should be interpreted as crack initiation lives rather than total fatigue lives. For severe corrosion defects, the propagation stage may contribute to the total remaining life, but it remains outside the scope of the present investigation.

3. Materials and Methods

The overall methodology is illustrated in Fig. 1. The procedure begins by defining the material properties and strain–life parameters for API 5L X65 steel. The FE framework is then benchmarked against a pit-corroded plate model reported in the literature. After validation, a three-dimensional quarter-pipe model containing an idealized rectangular corrosion defect is developed. The defect geometry, internal pressure, boundary conditions, and cyclic bending are specified according to the parametric design. A mesh convergence study is performed using the element length-to-thickness ratio to ensure reliable local stress–strain predictions. Nonlinear FE simulations are subsequently conducted to obtain the local cyclic stress–strain responses at the defect. Finally, the extracted local strain amplitude and maximum local stress are used in the CMB and SWT formulations to predict fatigue crack initiation life.

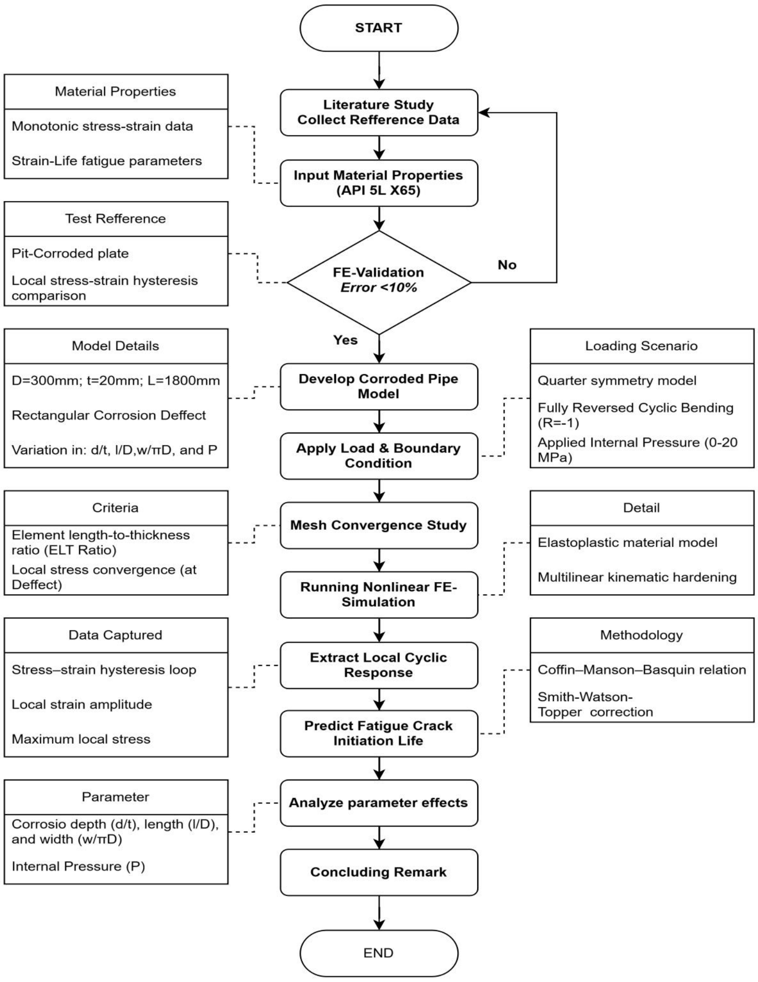

Figure 1. Flowchart of the research methodology used for strain–life fatigue assessment.

3.1. Material properties

API 5L X65 steel was used as the pipe material for both the benchmark validation and the parametric study. The mechanical properties include a yield strength (σ_y) of 464 MPa, an ultimate tensile strength (σ_{UTS}) of 563 MPa, an elastic modulus (E) of 210 GPa, and a Poisson's ratio of 0.3. The true stress–strain response from tensile testing is shown in Fig. 2a, while the strain–life parameters are shown in Fig. 2b. The material parameters were obtained from published data for API 5L X65 steel. The monotonic tensile properties, including the yield strength, ultimate tensile strength, elastic modulus, Poisson's ratio, and true stress–strain curve, were used to define the elastoplastic response of the material. The strain–life fatigue data were used to define the elastic and plastic strain components in the Coffin–Manson–Basquin relation to predict fatigue crack initiation.

For the finite element analysis, the cyclic elastoplastic response of API 5L X65 steel was represented using a multilinear kinematic hardening model. The available true stress–strain data were converted to true stress–plastic strain data and used to define the corresponding multilinear hardening points in ANSYS Mechanical. Kinematic hardening was selected because it can represent the yield-surface translation during reversed loading. This feature is important for cyclic bending simulations because the stress state repeatedly changes between tensile and compressive loading, particularly near the corrosion defect, where local elastoplastic deformation occurs. Therefore, the calibrated multilinear kinematic hardening model was used to capture the cyclic stress–strain response required for the strain–life fatigue assessment. In the present framework, monotonic stress–strain data were used to define the nonlinear elastoplastic response in the finite element model, whereas strain–life parameters were used during fatigue post-processing to calculate crack initiation life from the extracted local cyclic strain response.

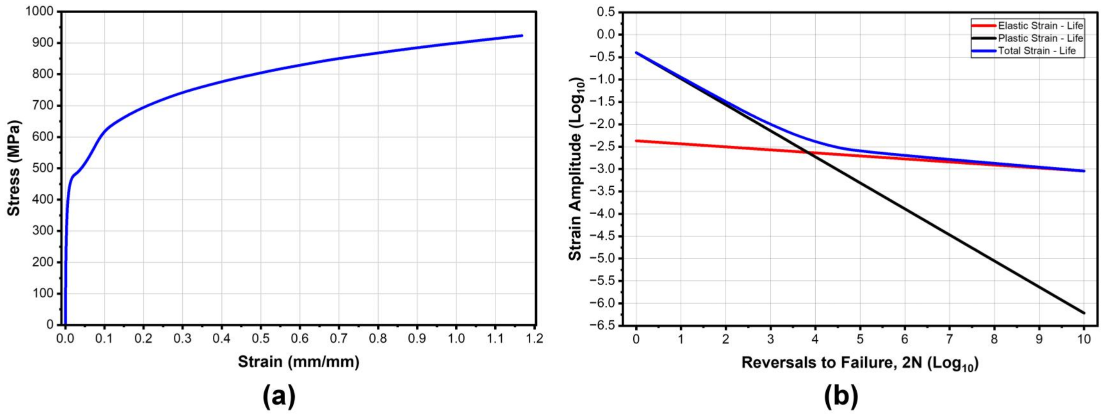

Figure 2. Material properties of API 5L X65 steel: (a) true stress–strain curve (Lo, Karuppanan and Ovinis, 2022); (b) strain–life curve used for fatigue-life prediction (the plotted graph is based on fatigue data parameters obtained from Farhad *et al.*, (2019); and Härkegård and Mann, (2003)).

3.2. FE model validation

The finite element framework used in this study was validated through a benchmark simulation of the pit-corroded plate reported by Farhad *et al*. (2019). The benchmark was reproduced in ANSYS Workbench using API X65 steel. The pit geometry and boundary conditions are shown in Figs. 3 and 4.

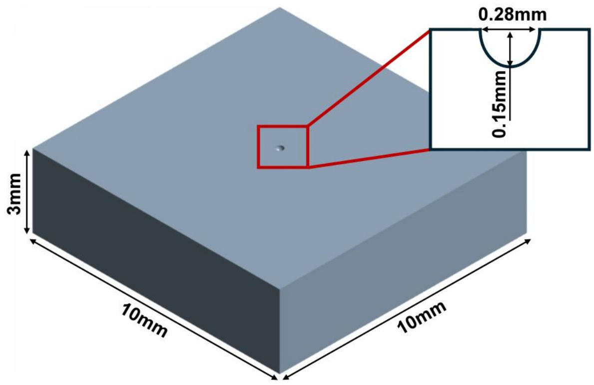

Figure 3. Geometry of the pit-corroded plate benchmark model.

The geometric configuration affects mesh topology, particularly in regions of high stress concentration. Therefore, element quality was evaluated prior to analysis using standard metrics, including the Jacobian ratio, skewness, and aspect ratio, to ensure numerical stability in nonlinear cyclic plasticity simulations (Prabowo *et al.*, 2019; Ilyin and Pronina, 2025). The reference model was discretized using a multizone meshing technique, resulting in a hex-dominant mesh with 162,658 nodes and 74,145 elements, as shown in Fig. 4. The mesh exhibited an average Jacobian ratio of 0.996, skewness of 0.443, and an aspect ratio of 5.02, indicating acceptable element quality for nonlinear cyclic plasticity analysis.

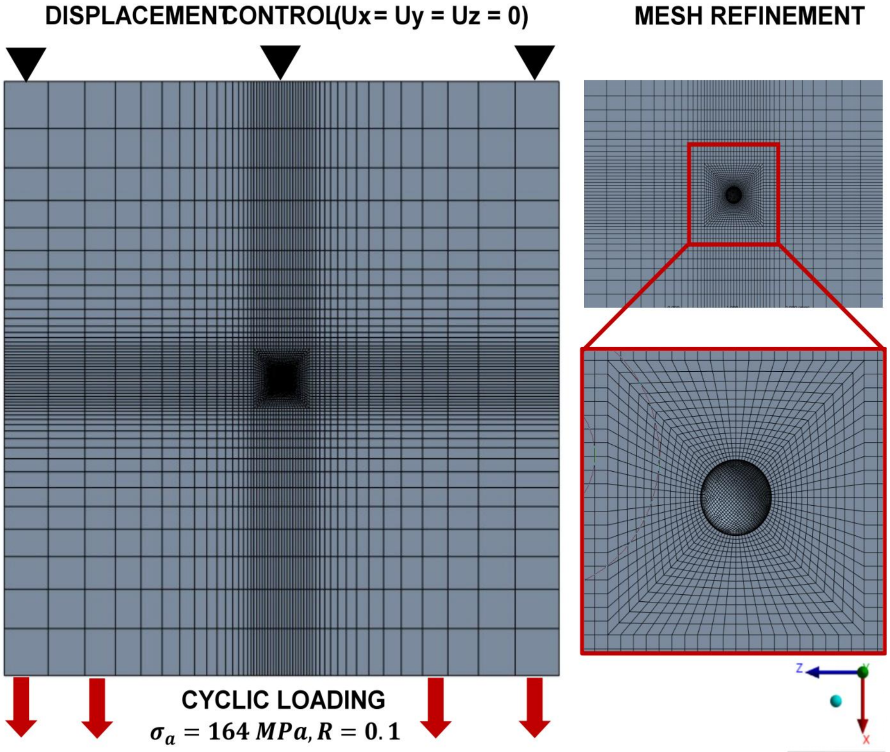

Figure 4. Boundary conditions and meshing strategy used for the benchmark model.

Monotonic tensile loading was first applied to establish the initial local stress–strain field and identify the critical region around the pit. The cyclic loading condition was defined by a stress amplitude of 164 MPa and a stress ratio of $R = 0.1$. The stress ratio is defined as the ratio between the minimum and maximum stresses in a single loading cycle, as given in Eq. (5). The maximum cyclic stress was calculated from the stress amplitude using Eqs. (6) and (7), yielding a value of approximately 364 MPa. During the monotonic step, the tensile load was ramped from zero to this maximum stress to establish the local stress–strain contours and define the initial state for cyclic loading, as shown in Figs. 5 and 6.

$$R = \frac{\sigma_{min}}{\sigma_{max}} \tag{5}$$

$$\sigma_a = \frac{\sigma_{max} - \sigma_{min}}{2} \tag{6}$$

$$\sigma_{max} = \frac{2\sigma_a}{1-R} \tag{7}$$

The loading was then switched to cyclic conditions, with the applied stress varying between approximately 36 MPa and 364 MPa. The stress–strain response at the pit region was extracted to construct the corresponding hysteresis loops. The predicted hysteresis response agrees well with the reference results, as shown in Fig. 7. Minor quantitative differences may be attributed to variations in meshing strategy, material implementation, and solver algorithms. Given the nonlinear nature of cyclic plasticity, this level of agreement is acceptable for fatigue analysis.

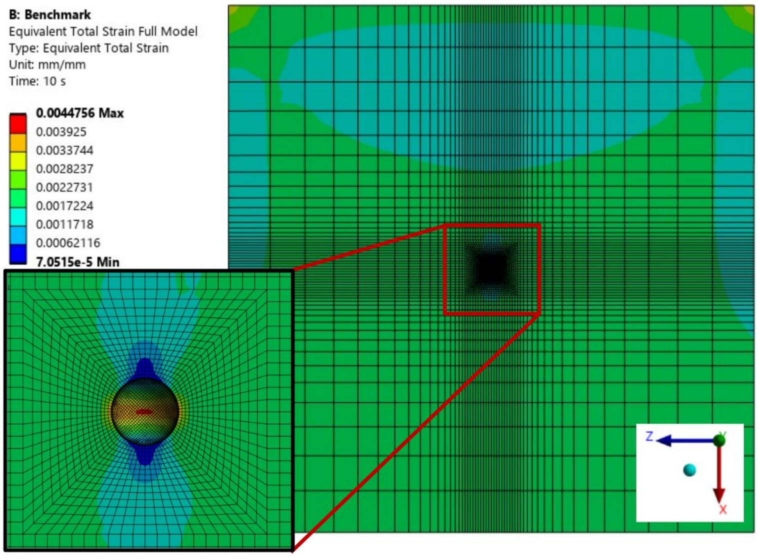

Figure 5. Strain contour of the full benchmark model under monotonic loading.

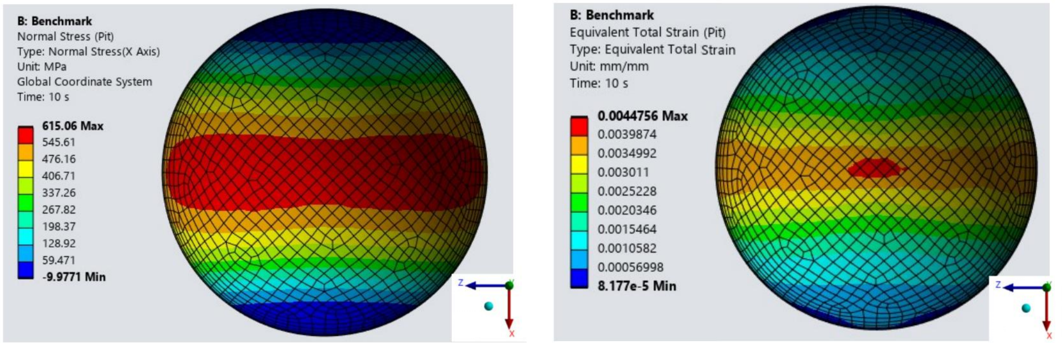

Figure 6. Stress and strain contours around the corrosion pit.

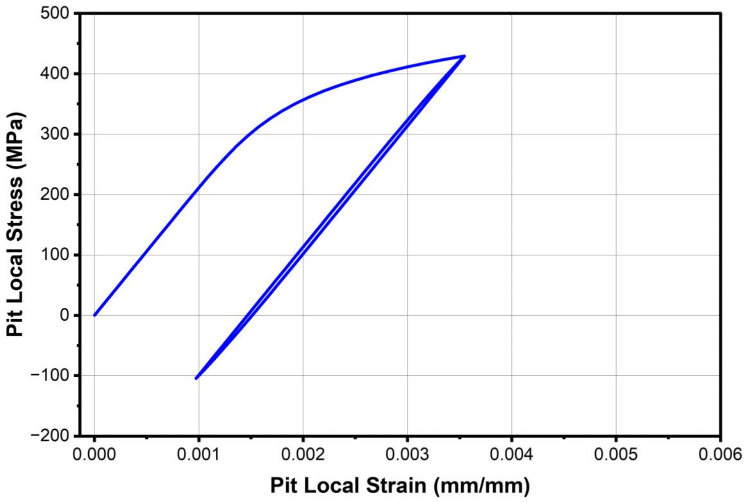

Figure 7. Hysteresis response obtained in the present study (for comparison, see Farhad *et al.* (2019)).

Overall, the validation focused on the local cyclic stress–strain response around the corrosion pit, which is the principal input for the strain–life (ε–N) fatigue assessment. The good agreement between the hysteresis loops indicates that the adopted material model, nonlinear cyclic plasticity formulation, meshing strategy, and local response extraction procedure can reasonably reproduce the local elastoplastic behavior at corrosion defects. However, the benchmark geometry is a pit-corroded flat plate; therefore, it does not fully represent pipeline curvature, hoop stress, or the interaction between global bending and internal pressure. The validation should therefore be interpreted as verification of the local cyclic plasticity response and fatigue-parameter extraction procedure, rather than full validation of pipeline-scale behavior. Direct experimental validation of the full corroded pipe model was not performed in this study. As a result, the absolute fatigue-life estimation should be interpreted with caution, while the predicted trends are more reliable for identifying governing mechanisms. Future work should include experimental validation using corroded pipe specimens subjected to combined internal pressure and cyclic bending.

3.3. Model geometry and defect parameters

The rectangular corrosion defect used in this study is illustrated in Fig. 8, and the corresponding geometric parameters are summarized in Table 1. The pipe model has an outer diameter of 300 mm, a wall thickness of 20 mm, and a total length of 1,800 mm. The defect geometry was varied in terms of normalized depth, length, and width to evaluate the individual effects of each parameter on the local fatigue response (Prabowo *et al.*, 2022; Hanif *et al.*, 2023; Pratama *et al.*, 2023; Capula-Colindres *et al.*, 2024). The selected parameter ranges cover severe corrosion conditions and were used to investigate fatigue sensitivity rather than to represent typical service defects.

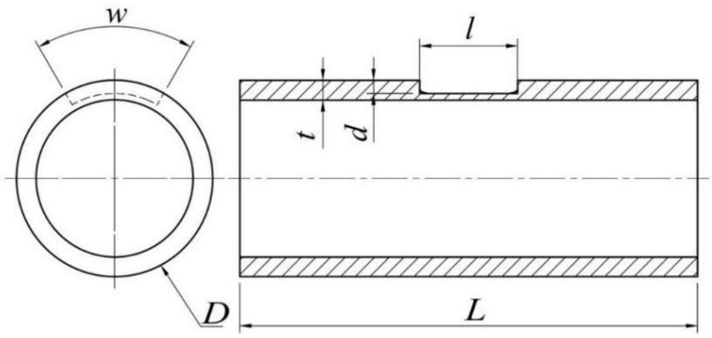

Figure 8. Definition of the corrosion defect.

Table 1. Corrosion defect parameters

No	Parameter	Value
1	Overall length (L) in mm	1,800
2	Diameter (D) in mm	300
3	Wall thickness (t) in mm	20
4	Normalized corrosion depth (d/t)	0.1 – 0.8
5	Normalized corrosion length (l/D)	0.25 – 2.0
6	Normalized corrosion width $(w/\pi D)$	0.1 – 0.4
7	Internal pressure (P) in MPa	0 – 20

Actual corrosion defects in subsea pipelines are often irregular and may involve pit clustering, nonuniform wall thinning, and rough defect boundaries. Nevertheless, engineering assessment procedures commonly characterize metal-loss defects using measurable geometric parameters, such as defect depth and longitudinal extent, as reflected in DNVGL-RP-F101 (DNV GL, 2017). In this study, the rectangular defect was adopted as an idealized representation of localized metal loss to support a systematic parametric investigation. This simplified geometry allows corrosion depth, length, and width to be controlled independently and compared directly. Therefore, the rectangular defect should be interpreted as a controlled idealization for identifying fatigue mechanisms associated with local wall thinning, rather than as an exact representation of actual corrosion morphology. Future work may extend the present framework by incorporating irregular corrosion profiles from inspection data or stochastic defect models.

3.4. Boundary conditions and meshing strategy

The numerical simulations were conducted using a three-dimensional quarter-pipe model, as shown in Fig. 9, to reduce computational cost while preserving the structural response of the full geometry. Symmetry boundary conditions were applied to the axial and circumferential symmetry planes, where the normal displacement component was constrained, and the tangential components were left free. The corrosion defect was centered with respect to the symmetry planes; therefore, the deformation and the resulting plastic zone were assumed to remain symmetric, and the reduced model represented the full pipe response.

The pipe was subjected to combined cyclic bending and internal pressure. Displacement-controlled rotation was applied at the pipe end to generate the prescribed bending moment, while the internal pressure was uniformly distributed over the inner surface. The loading history consisted of a fully reversed cyclic rotational displacement with a rotation amplitude of 0.2 rad under quasi-static conditions. The selected rotation amplitude was not intended to represent a specific operational loading condition. Instead, it was used to generate sufficient cyclic deformation to activate local elastoplastic behavior at the corrosion defect. This approach enables the strain–life fatigue framework to capture the strain-controlled damage mechanism governing crack initiation in the defect region. Thus, it served as a controlled comparative loading condition for the parametric study rather than as a calibrated representation of a particular offshore loading event.

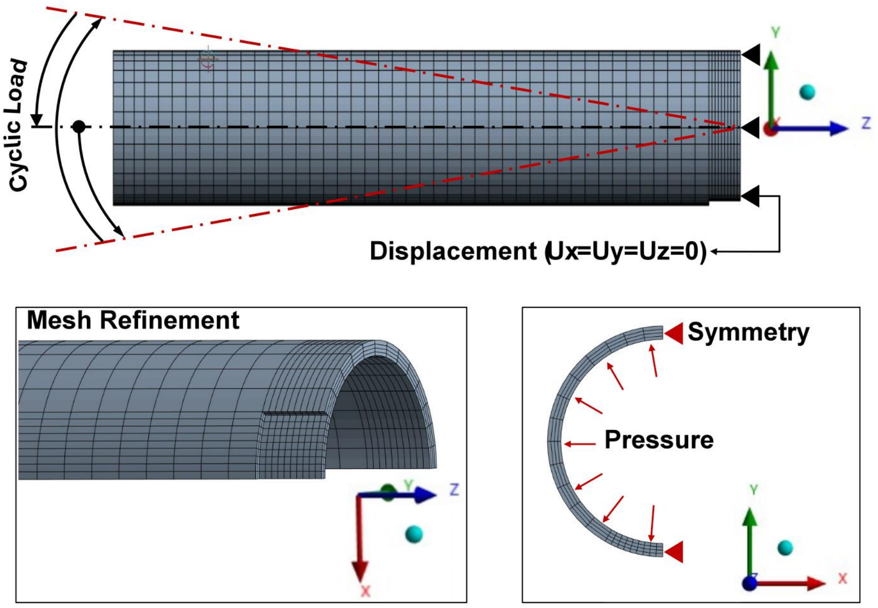

Figure 9. Applied Boundary Conditions

A mesh convergence study was first conducted on a representative configuration to determine an appropriate mesh density for the numerical analysis, considering both numerical accuracy and computational efficiency (Riffat *et al.*, 2025; Samaei and Ghahfarokhi, 2025). In this procedure, a single corrosion geometry was discretized using progressively refined three-dimensional hexahedral meshes. For each mesh configuration, a simplified loading condition was applied, and the maximum equivalent von Mises stress in the defect region was monitored as the convergence indicator.

Fig. 10 presents the variation in the normalized maximum equivalent stress as a function of the element length-to-thickness (ELT) ratio (Eq. 8) (Alsos and Amdahl, 2007; Haris and Amdahl, 2013; Prabowo *et al.*, 2023).

$$ELT = \frac{l_e}{t_{ef}} \tag{8}$$

The element length (l_e) is defined as the characteristic in-plane dimension of the surface element within the axial–circumferential plane of the pipe. For non-square elements, the larger in-plane dimension is conservatively adopted to define the ELT ratio. To prevent numerical distortion and ensure reliable stress–strain predictions, the in-plane aspect ratio of elements in the defect region was maintained below 3 throughout the analysis. For intact regions, the effective thickness is equal to the nominal pipe-wall thickness ($t_{ef} = t$). However, in corroded regions, the effective thickness is reduced by the corrosion depth ($t_{ef} = t - d$).

The convergence results indicate that for ELT values between 5 and 9, the predicted maximum equivalent stress becomes essentially insensitive to further mesh refinement. For larger ELT values, noticeable deviations in stress prediction are observed. Conversely, excessively refined meshes yield only marginal changes in stress results while significantly increasing computational time. Therefore, an ELT range of 5–9 was identified as providing an optimal compromise between numerical accuracy and computational efficiency. This ELT range was subsequently adopted as a mesh design criterion for all other corrosion configurations analyzed in this study.

Since the corrosion severity varied from 0.1 to 0.8, the local effective thickness changed accordingly for each analysis case. Rather than performing a separate convergence study for each corrosion case, the in-plane element size in the defect region was adjusted to keep the ELT ratio within the previously established converged range. This approach ensured consistent mesh resolution relative to the structural thickness while avoiding redundant convergence analyses for each parameter variation.

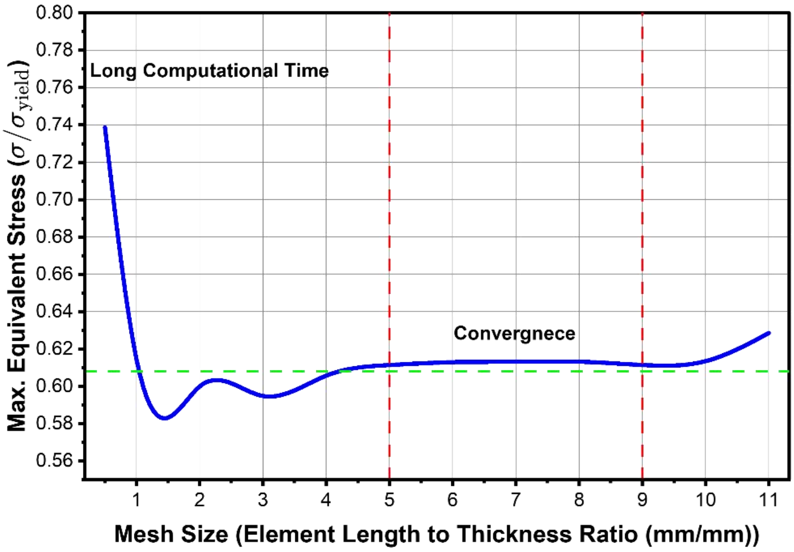

Figure 10. Mesh convergence based on normalized maximum von Mises stress vs the ELT ratio.

The mesh-convergence study based on the ELT ratio served as the primary numerical sensitivity assessment in this work. Uncertainty in the fatigue material parameters and prescribed loading amplitude should also be considered when interpreting the predicted fatigue lives. The Coffin–Manson–Basquin and SWT relations are nonlinear; therefore, relatively small changes in the local strain amplitude, maximum stress, or fatigue coefficients may produce substantially larger changes in the absolute crack-initiation life. Similarly, a change in the imposed rotation amplitude would directly modify the local strain amplitude at the corrosion defect and, consequently, the calculated fatigue life. A dedicated probabilistic or parametric sensitivity analysis was not performed in the present study. Therefore, the reported fatigue lives should be interpreted as deterministic comparative estimates for the specified material data and loading conditions, whereas the relative trends in corrosion depth, length, width, and internal pressure are considered more robust.

3.5. FE solver and analysis procedures

All finite element simulations were performed in ANSYS Workbench using the ANSYS Mechanical implicit solver. A nonlinear static structural analysis was conducted to capture the elastoplastic material response. Material nonlinearity was represented using a multilinear kinematic hardening model, which is suitable for reversed cyclic loading. The applied loads consisted of constant internal pressure and cyclic bending. Both loads were applied incrementally under quasi-static conditions to obtain the local cyclic stress–strain response at the corrosion defect. Dynamic effects and inertia were neglected because the analysis focused on fatigue crack initiation under slowly varying cyclic deformation rather than transient structural response.

The cyclic bending load was defined with a nominal stress ratio $R = -1$, corresponding to fully reversed bending with an approximately zero nominal mean stress. However, the fatigue assessment was based on the local stress–strain response obtained from the FE simulation, rather than on the nominal bending condition alone. When internal pressure was applied, the pressure-induced tensile membrane stress was superimposed on the cyclic bending stress. As a result, the local stress cycle at the corrosion defect shifted toward a non-zero tensile mean stress, even though the nominal bending load remained fully reversed.

The internal pressure was therefore treated as a constant static load during cyclic bending. It did not contribute to the alternating bending component, but it increased the local maximum stress and mean stress at the defect region. This effect became more pronounced in corroded regions because the reduced wall thickness amplified the local pressure-induced stress. The extracted local cyclic response was subsequently used to predict fatigue crack initiation life, as described in Section 3.6.

3.6. Fatigue-life extraction and modeling assumptions

Fatigue-life predictions were performed during post-processing using the local cyclic stress–strain responses obtained from nonlinear FE simulations. For each corrosion configuration, the stress and strain histories were extracted from the critical element at the corrosion defect, identified by the maximum local strain response. The stress–strain response was monitored during repeated loading increments until the hysteresis loop stabilized. The stabilized cycle was then used to determine the local total strain amplitude and maximum local stress.

The Coffin–Manson–Basquin relation was used as the primary strain–life formulation for fatigue crack initiation prediction. When internal pressure produced a non-zero local tensile mean stress, the Smith–Watson–Topper parameter was applied to account for the combined effects of local strain amplitude and maximum tensile stress. The extracted local strain amplitude and maximum local stress were substituted into the strain–life equations to obtain the number of reversals to failure, which was then converted into cycles to fatigue crack initiation. The predicted fatigue lives should be interpreted as comparative estimates of crack initiation under the prescribed numerical conditions. Effects of crack propagation, corrosion growth, residual stress, welds, variable-amplitude loading, and environmental degradation during cycling were not included in the present formulation.

4. Results and Discussion

4.1. Local strain-controlled fatigue mechanism

The results are discussed in terms of how each parameter modifies the local cyclic strain state at the corrosion defect. Fig. 11 compares the strain distribution in intact and corroded pipelines. The intact pipe shows a relatively uniform strain field, indicating that deformation is mainly governed by the global structural response. In contrast, the corroded pipe shows pronounced strain localization at the defect region, indicating that local wall thinning changes the deformation pattern from global to local behavior. This localization occurs because corrosion reduces the local wall thickness and introduces a geometric discontinuity. Under cyclic bending, the intact pipe distributes deformation along the pipe wall. In the corroded pipe, however, the reduced local stiffness concentrates bending deformation around the defect. Consequently, the local cyclic strain amplitude increases near the deepest region of the defect and around the transition between the intact and thinned wall regions.

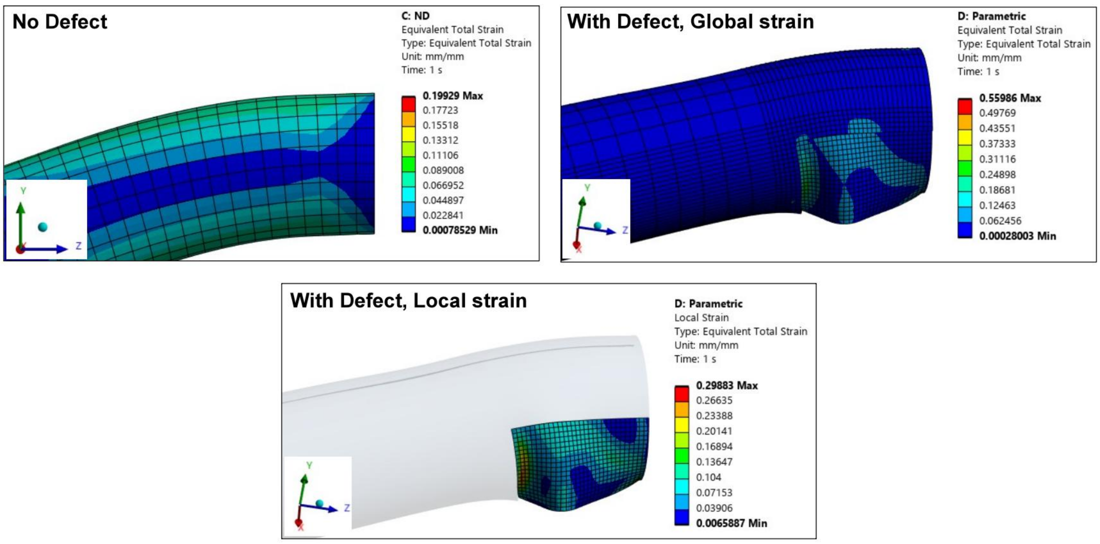

Figure 11. Comparison of strain distribution in intact and corroded pipes under monotonic loading (d/t = 0.4; l/D = 2.0; $w/\pi D$ = 0.4; and P = 10 MPa)

The cyclic response in Fig. 12 confirms that the defect region undergoes elastoplastic deformation. The stabilized hysteresis loops show a clear enclosed area, representing local plastic strain energy dissipated during cyclic loading. This response indicates that the material behavior at the defect is not purely elastic. Therefore, nominal-stress-based assessment alone is insufficient; fatigue crack initiation should be evaluated using the local cyclic strain amplitude, the governing parameter in the strain–life framework.

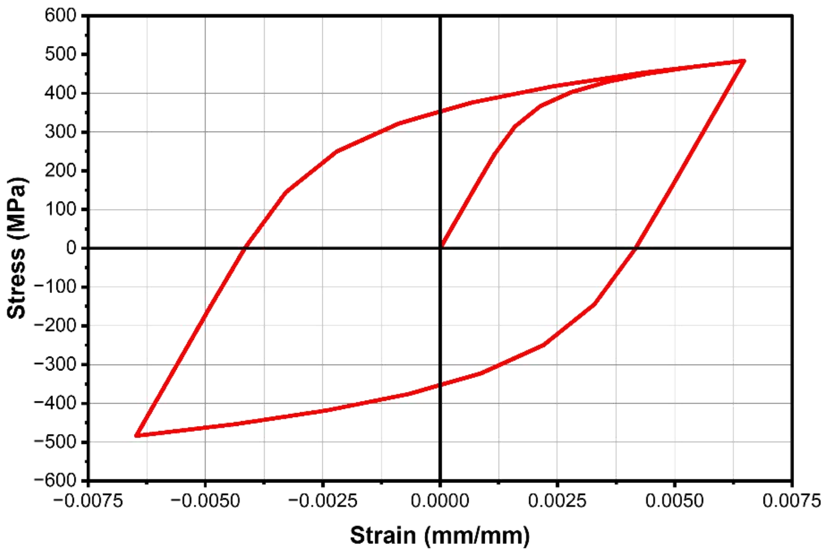

Figure 12. Hysteresis loops during cyclic bending at the corrosion defect.

Fig. 13 further shows the direct relationship between strain localization and fatigue damage. The minimum fatigue life and maximum fatigue damage occur at the defect region, where the local strain concentration is highest. This confirms that fatigue crack initiation is expected to occur at the corrosion defect rather than in the nominally intact pipe wall. Thus, the fatigue performance of the corroded pipeline is controlled by the local mechanical response at the defect.

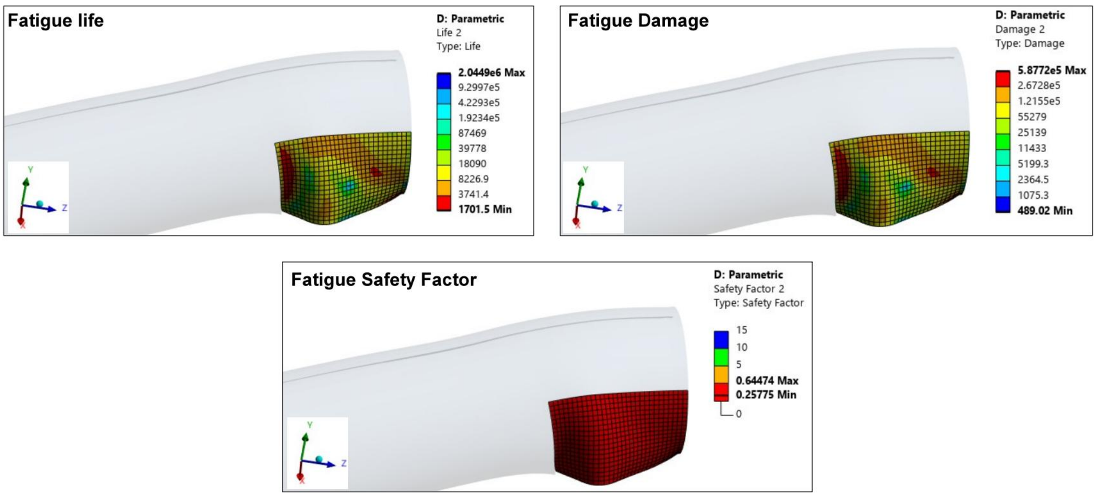

Figure 13. Fatigue life, fatigue damage, and fatigue safety factor at the defect region (d/t = 0.4; l/D = 2.0; $w/\pi D$ = 0.4; and P = 10 MPa)

Based on these observations, fatigue in the corroded pipeline is interpreted as a local strain-controlled mechanism. Corrosion geometry and internal pressure affect fatigue life by modifying the local cyclic strain amplitude, the extent of elastoplastic deformation, and the local mean stress at the defect. The following subsections therefore discuss each parameter according to its specific influence on the local strain field and the resulting fatigue crack initiation life.

4.2. Effect of corrosion length on fatigue life

Fig. 14 shows that the predicted fatigue life increases with corrosion length within the investigated range. This trend may appear counterintuitive because a larger defect is commonly associated with lower structural integrity. However, in the strain–life framework used here, crack initiation is governed primarily by the local cyclic strain amplitude at the critical location rather than by defect size alone. For short corrosion defects, the metal-loss region behaves as a localized geometric discontinuity. Deformation is strongly constrained around the defect, which produces a high strain concentration.

Under displacement-controlled bending, the imposed curvature is accommodated over a small region, resulting in a large plastic strain amplitude and rapid accumulation of fatigue damage.

As the corrosion length increases, the response shifts from localized, notch-like behavior to more distributed wall thinning. Bending deformation spreads over a longer corroded region, thereby reducing local constraint and lowering the peak cyclic strain at the critical point. Although the damaged area becomes larger, the local strain concentration decreases. Since the strain–life relation is highly sensitive to strain amplitude, this reduction in peak strain leads to a longer predicted crack initiation life. This result indicates a transition from notch-controlled fatigue in short defects to fatigue governed by distributed wall thinning in longer defects.

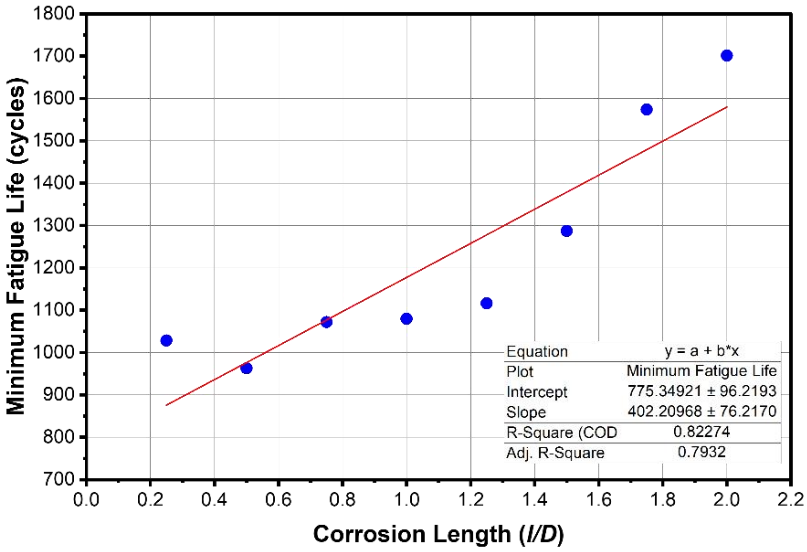

Figure 14. Effect of corrosion length on predicted fatigue crack-initiation life (d/t = 0.4; $w/\pi D$ = 0.4; and P = 10 MPa)

This trend should not be interpreted as evidence that corrosion is beneficial. Rather, it shows that fatigue crack initiation under the present displacement-controlled condition is controlled by strain localization, not by corrosion length alone. Therefore, corrosion geometry should be evaluated through its effect on the local strain field. This trend is specific to the strain-based assessment under displacement-controlled bending. Under nominal stress-controlled conditions, a different trend may occur because the remaining net-section area becomes more influential. Thus, the present result does not contradict conventional understanding of fatigue; instead, it reflects the difference between stress-controlled and strain-controlled fatigue mechanisms.

4.3. Effect of corrosion depth on fatigue life

Fig. 15 shows the effect of corrosion depth on the predicted minimum fatigue life. Fatigue life decreases markedly as the corrosion depth increases. The reduction is nonlinear: fatigue life drops rapidly at shallow to moderate depths, while the curve approaches a lower plateau at greater depths. This trend indicates that corrosion depth has a strong influence in the early stage of wall-thickness reduction, but its incremental effect diminishes once the defect becomes severe. Mechanically, increasing corrosion depth directly reduces the effective wall thickness at the defect. Under cyclic bending, this thickness reduction increases local compliance and amplifies bending strain near the corroded region. As a result, the local cyclic strain amplitude rises significantly. Because the present assessment is based on the strain–life framework, this increase in local strain amplitude accelerates fatigue damage accumulation and shortens the predicted crack initiation life.

The plateau-like behavior at larger depths can be attributed to the dominance of localized plastic deformation. Once the remaining wall becomes sufficiently thin, the material response is already governed by high plastic strain amplitude. Further increases in depth, therefore, do not produce a proportional increase in peak strain. Consequently, the predicted fatigue life approaches the lower bound set by the material's local cyclic plasticity capacity. These results confirm that corrosion depth is the most critical geometric parameter in the present strain-based assessment. Unlike defect length or width, which mainly affect strain redistribution, corrosion depth directly controls the remaining wall thickness and the magnitude of local cyclic deformation at the critical location.

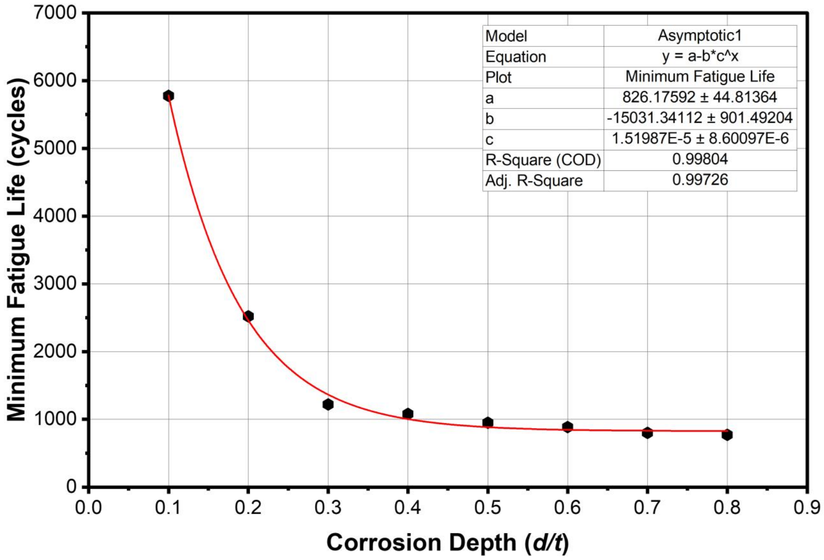

Figure 15. Effect of corrosion depth on predicted fatigue crack-initiation life (*l/D* = 1.0; *w/πD* = 0.4; and *P* = 10 MPa)

4.4. Effect of corrosion width on fatigue life

Fig. 16 shows the effect of corrosion width on the predicted fatigue life. Fatigue life decreases as the corrosion width increases, although the influence is much weaker than that of corrosion depth. The reduction is more noticeable at smaller widths, whereas the fatigue life tends to approach an approximately constant value at larger widths. Unlike corrosion depth, corrosion width does not directly reduce the remaining wall thickness. Instead, it modifies the circumferential constraint around the defect. For narrow defects, the surrounding intact wall provides strong restraint, which limits the extent of deformation in the thinned region. As the defect becomes wider, this restraint decreases, and a larger circumferential portion of the thinned wall participates in bending deformation. This increases the local cyclic strain amplitude and reduces the predicted fatigue life. When the defect becomes sufficiently wide, the local response stabilizes because the strain field within the defect region becomes more uniform. Further widening, therefore, produces only a small change in peak strain, leading to the plateau-like trend shown in Fig. 16.

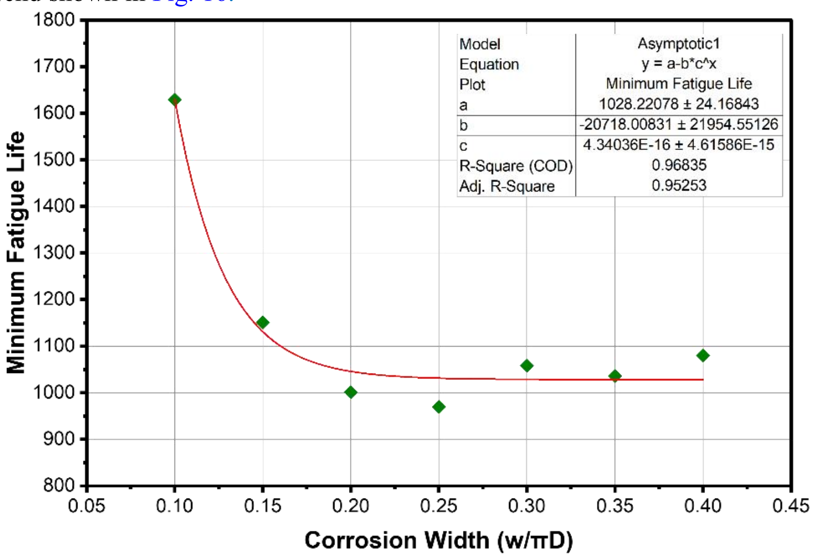

Figure 16. Effect of corrosion width on predicted fatigue crack-initiation life (*d/t* = 0.4; *l/D* = 1.0; and *P* = 10 MPa)

These results indicate that corrosion width is a secondary geometric parameter in the present strain-based fatigue assessment. It affects fatigue life by altering circumferential constraint and strain redistribution, but it does not control local cyclic deformation as directly as the corrosion depth does. Therefore, its contribution to fatigue degradation is more limited than that of wall-thickness reduction.

4.5. Effect of internal pressure on fatigue life

Fig. 17 shows the effect of internal pressure on the predicted fatigue life. Fatigue life decreases almost linearly with increasing internal pressure. This indicates that internal pressure is a detrimental loading parameter that accelerates fatigue damage in the corroded pipeline. Although cyclic bending was applied under fully reversed conditions ($R = -1$), internal pressure introduced a tensile membrane stress in the pipe wall. This stress was superimposed on the cyclic bending stress, resulting in a nonzero local mean stress at the corrosion defect. Therefore, the fatigue driving force was governed by the combined local stress state rather than by the nominal bending stress ratio alone. This behavior can be explained by stress superposition. Fully reversed bending produces alternating tensile and compressive stresses with approximately zero nominal mean stress. In contrast, internal pressure produces a non-reversing tensile membrane stress. The local stress at the defect is therefore the sum of the cyclic bending stress and the constant pressure-induced membrane stress. As pressure increases, both the local mean stress and maximum stress during each cycle increase. This effect is amplified in the corroded region because the reduced wall thickness increases the local pressure-induced stress. Within the strain–life framework, this mean-stress effect was accounted for using the SWT parameter. Increasing internal pressure raises the maximum local tensile stress, thereby increasing the SWT damage parameter. As a result, the predicted fatigue crack initiation life decreases.

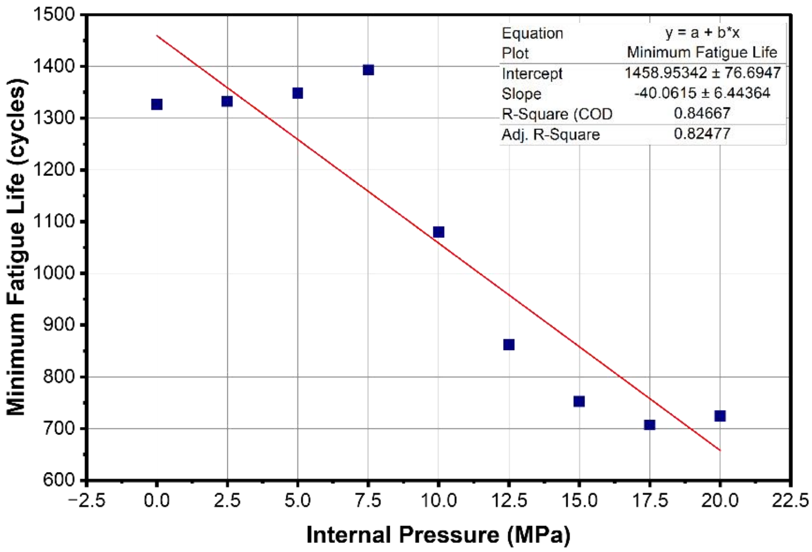

Figure 17. Effect of internal pressure on predicted fatigue crack-initiation life (d/t = 0.4; l/D = 1.0; and $w/\pi D$ = 0.4)

The use of the SWT criterion is therefore appropriate for the combined loading condition considered in this study. Without internal pressure, fully reversed bending produces approximately zero nominal mean stress. When pressure is applied, however, the local stress cycle shifts toward the tensile region. Because the SWT parameter includes both maximum local stress and strain amplitude, it captures the detrimental effect of pressure-induced tensile mean stress on crack initiation. Mechanically, internal pressure increases the local mean stress and the maximum cyclic stress, promoting earlier crack initiation and faster fatigue damage accumulation. Thus, even under nominally fully reversed bending, the corroded pipe experiences a more severe fatigue condition when pressurized. These results show that internal pressure is a key operational parameter affecting fatigue performance. Unlike corrosion geometry, which primarily modifies the strain distribution, internal pressure directly increases the local mean stress and the maximum cyclic stress. Consequently, it reduces the fatigue resistance of corroded pipelines.

5. Conclusions

A numerical strain–life fatigue assessment was conducted for corroded subsea pipelines subjected to cyclic bending and internal pressure using nonlinear finite element analysis. Based on the results, the following conclusions can be drawn:

- Fatigue crack initiation is governed by the local cyclic strain response at the corrosion defect rather than by the nominal global stress or deformation of the pipe. The critical region occurs at the defect, where strain localization is most pronounced.

- Corrosion depth is the most influential geometric parameter. Increasing depth reduces the effective wall thickness and amplifies the local cyclic strain amplitude, thereby significantly reducing fatigue life. At larger depths, the effect becomes asymptotic because the response is dominated by localized cyclic plasticity.
- Corrosion length affects fatigue life through strain redistribution. Short defects act as severe strain concentrators, whereas longer defects distribute deformation over a wider region, thereby reducing the peak cyclic strain under displacement-controlled bending. This trend reflects a transition from notch-controlled fatigue to distributed wall thinning and should not be interpreted as evidence that corrosion is beneficial.
- Corrosion width has a secondary influence on fatigue life. It modifies circumferential constraint and strain redistribution, but its effect is weaker than that of corrosion depth because it does not directly reduce the remaining wall thickness.
- Internal pressure reduces fatigue life by introducing tensile membrane stress and generating a non-zero local mean stress, even under fully reversed bending. This increases the SWT fatigue-damage parameter and accelerates crack initiation.
- Validation was limited to the local cyclic stress–strain response of a pit-corroded plate benchmark and did not include full-scale experiments on corroded pipelines. Therefore, the predicted fatigue lives should be interpreted as comparative crack-initiation estimates, pending validation through pipe-scale experiments.

The main contribution of this work is the integrated application of established strain–life fatigue tools to clarify the coupled mechanical roles of corrosion geometry and internal pressure in fatigue crack initiation in subsea CO_2 pipelines. Overall, the fatigue performance of corroded subsea CO_2 pipelines is governed by coupled mechanisms. Thickness reduction controls the strain magnitude, defect length controls strain localization, defect width controls circumferential constraint, and internal pressure controls the local mean stress. Reliable fatigue assessments should therefore consider these coupled effects rather than evaluating each parameter independently.

Acknowledgements

This research was funded by the Indonesian Endowment Fund for Education (LPDP) under the auspices of the Indonesian Ministry of Higher Education, Science and Technology, and administered through the EQUITY Program of Universitas Sebelas Maret. The funding was provided under the "International Research Network Program EQUITY THE Impact Rankings 2025" scheme, with Contract No. 3817/UN27/HK.02/2025, 4315/B3/DT.03.08/ 2025 and No. 84/UN27/KS/2025, as stated in the signed document with ID No. 4141.1/UN27.22/PT.01.03/2025. The authors gratefully acknowledge this financial and institutional support.

References

Alsos, H.S. and Amdahl, J. (2007) "On the resistance of tanker bottom structures during stranding," *Marine Structures*, 20(4), 218–237. https://doi.org/10.1016/j.marstruc.2007.06.001.

Baig, A.R. *et al.* (2025) "Comprehensive Insights into Carbon Capture and Storage: Geomechanical and Geochemical Aspects, Modeling, Risk Assessment, Monitoring, and Cost Analysis in Geological Storage," *Sustainability*, 17(19), 8619. https://doi.org/10.3390/su17198619.

Basquin, O.H. (1910) "The exponential law of endurance tests," *Proceedings of the American Society for Testing and Materials*, 10, 625–630.

Capula-Colindres, S. *et al.* (2024) "Mechanical behavior of X60 pipelines containing pitting corrosion defects based on finite element method," *Forces in Mechanics*, 16, 100278. https://doi.org/10.1016/j.finmec.2024.100278.

Coffin Jr., L.F. (1954) "A study of the effects of cyclic thermal stresses on a ductile metal," *Transactions of the American Society of Mechanical engineers*, 76(6), 931–950.

DNV GL (2017) *DNVGL-RP-F101: Corroded Pipelines.* Edition May 2017. Høvik: DNV GL AS.

Ezzati, M. *et al.* (2021) "Strain ratcheting failure of dented steel submarine pipes under combined internal pressure and asymmetric inelastic cycling," *Ocean Engineering*, 219, 108336. https://doi.org/10.1016/j.oceaneng.2020.108336.

Fajri, A. *et al.* (2026) "Assessment of risk, safety, hazard, and economic challenges of CCS pipeline and wellbore implementation: Exploring emerging achievements in 2010–2025," *Unconventional Resources*, 11, 100337. https://doi.org/10.1016/j.uncres.2026.100337.

Farhad, F., Zhang, X. and Smyth-Boyle, D. (2019) "Fatigue behaviour of corrosion pits in X65 steel pipelines," *Proceedings of the Institution of Mechanical Engineers, Part C: Journal of Mechanical Engineering Science*, 233(5), 1771–1782. https://doi.org/10.1177/0954406218776338.

Gao, B. *et al.* (2024) "Finite element analysis of the limit load of pipe bend with local wall-thinning defect under complex loads," *International Journal of Pressure Vessels and Piping*, 208, 105141. https://doi.org/10.1016/j.ijpvp.2024. 105141.

Hanif, M.I. *et al.* (2023) "Assessment of the ultimate strength of stiffened panels of ships considering uncertainties

in geometrical aspects: Finite element approach and simplified formula," *Ocean Engineering*, 286, 115522. https://doi.org/10.1016/j.oceaneng.2023.115522.
Haris, S. and Amdahl, J. (2013) "Analysis of ship-ship collision damage accounting for bow and side deformation interaction," *Marine Structures*, 32, 18–48. https://doi.org/10.1016/j.marstruc.2013.02.002.
Härkegård, G. and Mann, T. (2003) "Neuber prediction of elastic-plastic strain concentration in notched tensile specimens under large-scale yielding," *Journal of Strain Analysis for Engineering Design*, 38(1), 79–94. https://doi.org/10.1243/030932403762671917.
Ilyin, A. and Pronina, Y. (2025) "Curved pipes subjected to mechanochemical corrosion under pressure: Analytical and numerical estimates of the lifetime," *International Journal of Engineering Science*, 215, 104319. https://doi.org/ 10.1016/j.ijengsci.2025.104319.
Islami, D.P. *et al.* (2025) "Effects of crevice corrosion induced by biofouling on the mechanical response of engineered plate designs as an idealization of naval and marine structures," *Ocean Engineering*, 340, 122406. https://doi.org/10.1016/j.oceaneng.2025.122406.
Lo, M., Karuppanan, S. and Ovinis, M. (2022) "ANN- and FEA-Based Assessment Equation for a Corroded Pipeline with a Single Corrosion Defect," *Journal of Marine Science and Engineering*, 10(4), 476. https://doi.org/10.3390/jmse10040476.
Manson, S.S. (1953) *Behavior of materials under conditions of thermal stress*. NACA Technical Note 2933. Cleveland, OH: Lewis Flight Propulsion Laboratory, National Advisory Committee for Aeronautics.
Miner, M.A. (1945) "Cumulative Damage in Fatigue," *Journal of Applied Mechanics*, 12(3), A159–A164. https://doi.org/10.1115/1.4009458.
Prabowo, A.R. *et al.* (2022) "Forecasting the Effects of Failure Criteria in Assessing Ship Structural Damage Modes," *Civil Engineering Journal*, 8(10), 2053–2068. https://doi.org/10.28991/CEJ-2022-08-10-03.
Prabowo, A.R. *et al.* (2023) "Comparative study of shell element formulations as NLFE parameters to forecast structural crashworthiness," *Curved and Layered Structures*, 10(1), 20220217. https://doi.org/10.1515/cls-2022-0217.
Prabowo, A.R., Putranto, T. and Sohn, J.M. (2019) "Simulation of the Behavior of a Ship Hull under Grounding: Effect of Applied Element Size on Structural Crashworthiness," *Journal of Marine Science and Engineering*, 7(8), 270. https://doi.org/10.3390/jmse7080270.
Pratama, A.A. *et al.* (2023) "Hollow tube structures subjected to compressive loading: implementation of the pitting corrosion effect in nonlinear FE analysis," *Journal of the Brazilian Society of Mechanical Sciences and Engineering*, 45, 143. https://doi.org/10.1007/s40430-023-04067-3.
Riffat, J., Doudran, H.A. and Samaei, S.R. (2025) "AI-driven digital twin for uncertainty-aware structural health monitoring of offshore wind turbines considering biofouling effects and reliability prediction," *Green Technology & Innovation*, 1(2), 025330013. https://doi.org/10.36922/GTI025330013.
Riffat, J., Nazari, K. and Samaei, S.R. (2026) "AI-Driven Digital Twin Framework for Adaptive and Real-Time Structural Health Monitoring of Offshore Marine Structures," *Artificial Intelligence for Sustainable Cities*, 1(1), 90–104. https://doi.org/10.65582/aifsc.2026.006.
Riffat, J., Samaei, S.R. and Ghahfarokhi, M.A. (2025) "AI-Based Optimization and Hydrodynamic Performance of Floating Pontoon Breakwaters through Experimental and Numerical Modeling," *Global Decarbonisation*, 1(1), 1–26. https://doi.org/10.17184/eac.9847.
Samaei, S.R. and Ghahfarokhi, M.A. (2025) "Hydrodynamic Assessment of Floating Dock Behavior : A Case Study in Bahonar Port, Bandar Abbas," *Energy Catalyst*, 1(1), 104–112. https://doi.org/10.61552/EC.2025.008.
Talebi, M. *et al.* (2018) "Collapse of HSLA steel pipes under corrosion exposure and uniaxial inelastic cycling," *Journal of Constructional Steel Research*, 144, 253–269. https://doi.org/10.1016/j.jcsr.2018.02.003.
Udonsek, D.E., Tamonodukobipi, D. and Odokwo, V.E. (2023) "Corrosion-Based Integrity Analysis of Offshore Pipeline for Hydrocarbon Transportation," *Journal of Power and Energy Engineering*, 11(5), 24–41. https://doi.org/10.4236/ jpee.2023.115002.
Watson, P. and Topper, T.H. (1972) "Fatigue-damage evaluation for mild steel incorporating mean stress and overload effects," *Experimental Mechanics*, 12(1), 11–17. https://doi.org/10.1007/BF02320784.
Wennersten, R., Sun, Q. and Li, H. (2015) "The future potential for Carbon Capture and Storage in climate change mitigation – an overview from perspectives of technology, economy and risk," *Journal of Cleaner Production*, 103, 724–736. https://doi.org/10.1016/j.jclepro.2014.09.023.
Zhou, L. *et al.* (2025) "Evaluation on collapse behaviour of thick-walled pipes with corrosion defect under combined external pressure, axial tension and bending moment," *Structures*, 75, 108593. https://doi.org/10.1016/ j.istruc.2025.108593.
Zhou, L. *et al.* (2026) "Theoretical and numerical studies on collapse of corroded subsea pipelines under combined external pressure and axial tension," *Marine Structures*, 106, 103964. https://doi.org/10.1016/j.marstruc.2025.103964.